AGU
ADVANCING
EARTH AND
SPACE SCIENCE

Geophysical Research Letters

Key Points:
- Hyperspectral infrared radiances with high temporal resolution from geostationary (GEO) satellite provide four-dimensional (4D) wind fields
- The 4D wind fields can be extracted quantitatively with root mean squared error less than 2 m/s for U and V components of wind in troposphere against ERA5
- Higher temporal resolution from GEO measurements provides better wind profile information than lower temporal resolution

Correspondence to:
J. Li,
Jun.Li@ssec.wisc.edu

Four-Dimensional Wind Fields From Geostationary Hyperspectral Infrared Sounder Radiance Measurements With High Temporal Resolution

Zheng Ma[1,2,3] , Jun Li[2] , Wei Han[4] , Zhenglong Li[2] , Qingcun Zeng[1] , W. Paul Menzel[2] , Timothy J. Schmit[5] , Di Di[6], and Chian-Yi Liu[7,8]

[1]Institute of Atmospheric Physics, Chinese Academy of Sciences, Beijing, China, [2]Cooperative Institute for Meteorological Satellite Studies, University of Wisconsin-Madison, Madison, WI, USA, [3]University of Chinese Academy of Sciences, Beijing, China, [4]National Meteorological Center, China Meteorological Administration, Beijing, China, [5]Center for Satellite Applications and Research/ASPB, NOAA/NESDIS, Madison, WI, USA, [6]School of Atmospheric Physics, Nanjing University of Information Science and Technology, Nanjing, China, [7]Research Center for Environmental Changes, Academia Sinica, Taipei City, Taiwan, [8]Research Center for Space and Remote Sensing Research Center, National Central University, Taoyuan City, Taiwan

Abstract Four-dimensional (4D) wind fields were derived from radiance measurements of the Geosynchronous Interferometric Infrared Sounder (GIIRS) onboard the FengYun-4A satellite with 15-min temporal resolution during Typhoon Maria (2018). Results are evaluated with independent ERA5 reanalysis, Global Data Assimilation System (GDAS) analysis and dropsonde wind profiles, and show a statistical root mean squared error less than 2 m/s for U and V components in troposphere against ERA5 and GDAS. The temporal variation of the wind fields from GIIRS at 15-min intervals is consistent with that of the hourly ERA5. The added value of wind profiles over the numerical weather predictions (NWP) background field is also revealed. Further experiments confirm that higher temporal resolution from geostationary infrared (IR) sounder measurements could provide better dynamic information. 4D dynamic information can be extracted from high temporal resolution geostationary hyperspectral IR radiances in a consistent and continuous manner that can be used together with the thermodynamic information for various quantitative applications such as NWP data assimilation, near real-time weather monitoring, situational awareness and nowcasting.

Plain Language Summary A geostationary hyperspectral infrared (IR) sounder not only provides continuous observations of atmospheric thermodynamic information, but also provides continuous dynamic information critical for weather monitoring, warning, and forecast. The atmospheric motion vectors (AMVs) based on the geostationary imager observations using tracking techniques have been widely used in weather analysis and forecast. However, the retrieval of three-dimensional atmospheric wind fields from geostationary hyperspectral sounder measurements have not been well studied although a strong argument in favor of the realization of such an instrument has been the derivation of wind fields from moisture structures. The main reason is the lack of real observations from space. Using 15-min Geosynchronous Interferometric Infrared Sounder observations, an algorithm has been developed for deriving atmospheric four-dimensional (4D) wind fields, besides, the impacts of temporal resolution, cloudiness, and temporal information on 4D wind fields, respectively, are also studied. It indicates that both temporal and spatial information contributes to the 4D wind fields, and higher temporal resolution provides better 4D wind fields than the lower temporal resolution.

1. Introduction

Accurate four-dimensional (4D) wind observations are important contributors to atmospheric observation system and numerical weather predictions (NWP). With the help of geostationary meteorological satellites, algorithms to retrieve atmospheric motion vectors (AMVs) from continuous observations have been developed and optimized (Velden et al., 2005). The traditional methodologies are based on feature detection and tracking from three consecutive images. In cloudy skies, the visible and longwave infrared (IR) bands radiances can be used to track cloud motion-based vectors, while in clear skies water vapor sensitive band radiances are used for tracking moisture features for water vapor motion vectors. The derived AMVs have

been widely used in weather analysis and NWP data assimilation (Zhang et al., 2018; J. Li et al., 2020). Apart from target tracking methodologies, the optical flow methods based on image processing have also been applied to derive AMVs (Szantai et al., 2000, 2006), and recently were attempted to provide enhanced data sets from rapid-scan satellite imagers for mesoscale applications (Stettner et al., 2019; Sun et al., 2018). The largest source of uncertainty for AMVs from both methodologies is the height assignment (Velden & Bedka, 2009), and the temporal gaps during the extraction of AMVs also have a significant impact on the validness and accuracy of wind retrievals (García-Pereda & Borde, 2014).

With observations from hyperspectral IR sounders (Menzel et al., 2018), it is possible to solve the height assignment by tracking features in the retrieved water vapor profiles. For example, Santek et al. (2019) used moisture and ozone profiles retrieved from AIRS radiances to track three-dimensional (3D) AMVs over a high latitude region where consecutive observations occur with a polar orbiting satellite. The moisture retrieval error is the main source of uncertainties for 3D wind retrieval. However, such algorithm is not applicable for mid-to-lower latitudes due to a lack of sequential images from polar orbiting satellites.

The potential benefits of hyperspectral sounders onboard geosynchronous satellites on wind retrievals, by providing both sequential observations and detailed vertical profiles of moisture, have been studied via simulated data (Smith et al., 2002; Velden et al., 2004) Such measurements would potentially enhance the capability of forecasting severe storms (Schmit et al., 2009; Smith et al., 2009) such as tropical cyclones (TCs), deep convective, tornadic storms, etc., by providing key information on water vapor transportation both horizontally and vertically (especially in the boundary layer). Only advanced sounding missions from geostationary (GEO) orbit can provide the necessary high temporal and high spatial resolution 4D moisture and motion information. The "dwelling" nature of a 3-axis stabilized spacecraft in GEO orbit enables measurements with reduced noise and improved spatial resolution; this increases the yield of clear sky information (compared to that from a polar orbiting instrument). The World Meteorological Organization vision for global observing systems in 2040 suggests at least six geostationary satellites with advanced imagers and hyperspectral IR sounders (IRSs). EUMETSAT will have an advanced IRS in GEO orbit in 2023 (Holmlund et al., 2021); Japan is planning a GEO IRS for the Himawari-8/-9 follow-on (Okamoto et al., 2020).

The Geosynchronous Interferometric Infrared Sounder (GIIRS), which is the first advanced IRS onboard a GEO weather satellite, offers both high temporal and high-spectral resolution advanced sounder radiance measurements (Yang et al., 2017). It provides continuous monitoring of the fast-changing mesoscale environment relevant to severe weather nowcasting and forecasting (J. Li et al., 2011, 2012). In addition, it can improve local severe storm short-range forecast via regional NWP models with data assimilation (Z. Li et al., 2018; Yin et al., 2020), especially with an enhanced fast radiative transfer model (Di et al., 2018).

This study reports on an attempt to take advantage of the height assignment in 3D wind retrievals while avoiding the moisture retrieval uncertainty in GEO hyperspectral IRS measurements using a machine learning (ML) based retrieval methodology. ML is used for tracking the 4D wind field from two consecutive GIIRS high-spectral resolution brightness temperature (BT) observations with a temporal resolution of 15 min (note that the 15-min GIIRS data were only available during a special scan period of Typhoon Maria). Independent validation against ERA5, Global Data Assimilation System (GDAS) analysis, and dropsonde wind profiles indicate reasonable accuracy and precision. The temporal variation of the derived 4D wind field is consistent with ERA5; it is also found that higher temporal resolution data (e.g., 15 min compared to 30 min) provide better wind profile information. In addition, inclusion of spatial variances from four neighboring fields-of-view (FOVs) improves the 4D wind retrieval.

2. Data

GIIRS is a two-band hyperspectral IRS onboard the FengYun-4A (Yang et al., 2017), with long-wave (LW) IR band from 700–1,130 cm^{-1} (or 8.85–14.29 µm), mid-wave (MW) IR band from 1,650–2,250 cm^{-1} (or 4.44–6.06 µm), with sampled spectral resolution of 0.625 cm^{-1}. There are two observation modes of GIIRS; one is designed to scan China (4,500 × 4,500 km) with a temporal resolution of less than 1 h, the other is the mesoscale observing mode with temporal resolution of 30 min and coverage of 1,000 × 1,000 km. However, the GIIRS can also make special observations of an even smaller region with increased temporal resolution. During Typhoon Maria (2018), GIIRS made observations with a temporal resolution of 15 min, offering a

great opportunity for scientific study using high temporal resolution high-spectral resolution sounder measurements for retrieval and applications. As there exist some problems with the stability and spectral calibration of GIIRS measurements (Guo et al., 2021), the radiances used in this study are the re-sampled data generated by Space Science and Engineering Center of the University of Wisconsin-Madison, for which the spectral calibration error was used to re-sample the input radiances to provide more accurate spectral calibration.

Typhoon Maria was a powerful TC that affected Guam, the Ryukyu Islands, Taiwan, and East China in early July 2018. The typhoon reached its first peak intensity on July 6 and reached a second stronger peak intensity on July 9 with 10-min sustained winds of 195 km/h and a minimum pressure of 915 hPa. After crossing the Yaeyama Islands and passing north of Taiwan on July 10, Maria ultimately made landfall over Fujian, China, early on July 11, before dissipating. Maria produced heavy rains and strong winds across Taiwan, and impacted provinces of Fujian, Zhejiang, Jiangxi, and Hunan of China with flooding rain and gusty winds.

GIIRS made observations with an increased temporal resolution of 15 min on July 10 covering periods from 0000 to 1600 UTC, and 2100 to 2300 UTC. The target area was 13.7°–34.5°N, 108.9° to 136.2°E measured with a 96×68 array of squared FOVs with spatial resolution of around 16 km. For each hour there were four scans covering the whole area, starting at 00, 15, 30, and 45 min. Each scan lasted for 10-minutes, while the remaining 5 min were used for calibration. These intensive observations covered Typhoon Maria passing Taiwan and making landfall in mainland China.

Wind profiles from the ERA5 data set are used as benchmarks for the training process and validation of the retrieval output. The ERA5 reanalysis, generated by the European Centre for Medium-Range Weather Forecasts, has assimilated wind observations from in situ, radiosonde, dropsonde, aircraft measurements as well as AMVs from meteorological satellites (Hersbach et al., 2020), and has shown reliable accuracy in wind products against other reanalysis (Graham et al., 2019; Olauson, 2018; Taszarek et al., 2020). In this study, we employed the hourly gridded U-wind and V-wind data at 37 pressure levels from 1 to 1,000 hPa, with a spatial resolution of $0.25° \times 0.25°$. The U and V components of wind are interpolated to the time and location of individual GIIRS FOVs when used as true values for the training process, while no interpolation is performed for the independent validations.

3. Methodologies

3.1. GIIRS Channel Selection for Wind Profile Retrieval

To derive the wind profiles, it is important to select channels with less observation errors; the channels are selected based on the O-B (observed BT minus simulated BT from background) approach conducted offline, and those selected channels are then fixed in 4D wind field retrieval. Figure 1 shows the simulated GIIRS BT spectrum from U.S. Standard Atmosphere with selected channels (upper), the temperature Jacobian of LW selected channels (lower left), and the water vapor mixing ratio (lnq) Jacobians (lower right). It can be seen that the MW IR radiances are sensitive to water vapor changes at different atmosphere layers, which is the preliminary source of information for tracking the moisture-based wind profiles. Since, the LW IR radiances primarily provide the temperature profile information along with moisture information in boundary layer, they can also provide additional information for tracking the wind profile. Both GIIRS LW and MW channels are selected for tracking features, and the observations from LW FOVs are spatially matched-up to the location of MW FOVs based on the principle of shortest distance. As the predictors of the ML model include observations from the target FOV and the neighboring four FOVs surrounding it (top, bottom, left, and right), the ML retrievals are not very sensitive to the systematic mismatch in geolocation between LW and MW. As long as the five FOVs from both LW and MW have a good coverage of the target location and the neighboring area, the NN is able to apply appropriate relative weights and extract useful information from different FOVs.

3.2. Machine Learning Based Methodology for Wind Profile Retrieval

While previous methodologies on wind retrievals are mostly based on objective detection and tracking of movements, the new ML based algorithm developed in this study is training a feed-forward neuron
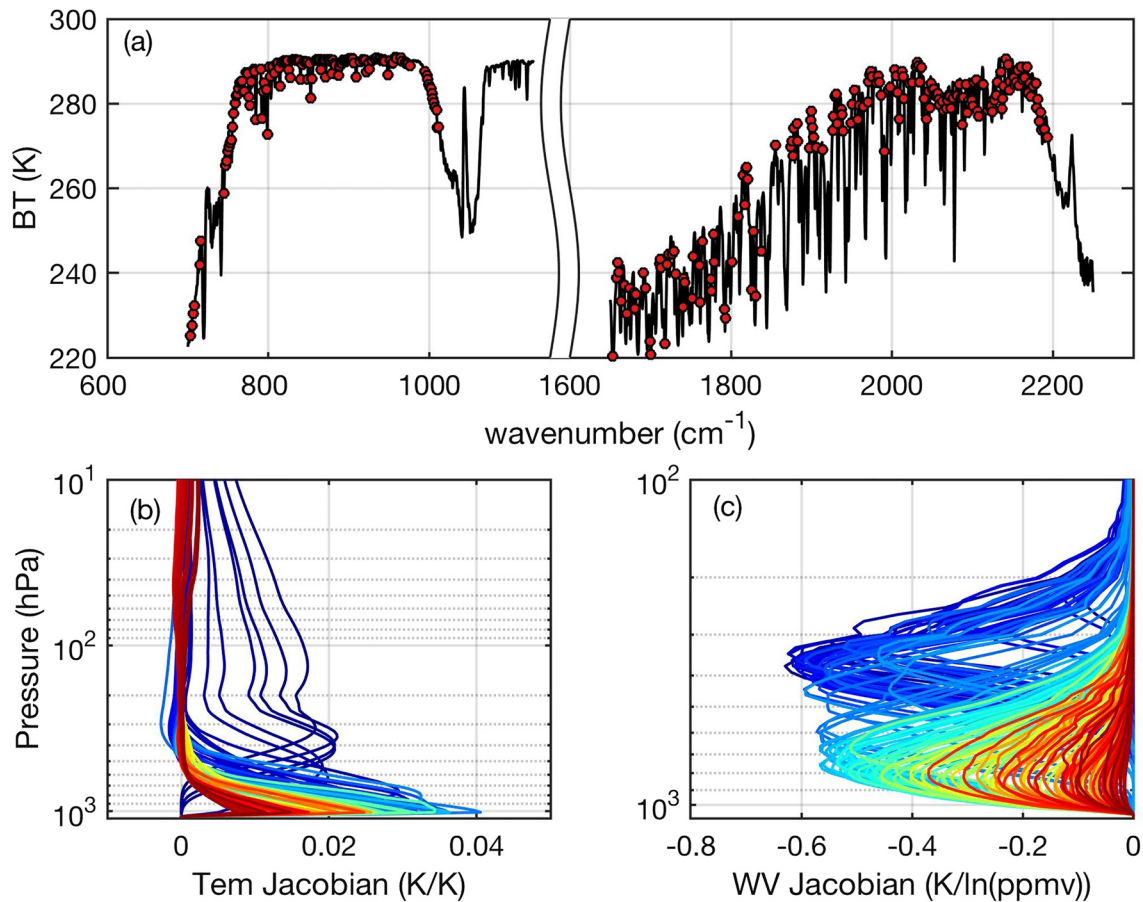
Figure 1. Simulated brightness temperature spectrum of Geosynchronous Interferometric Infrared Sounder from 1976 U.S. Standard Atmosphere with selected channels (upper), the temperature Jacobian of long-wave selected channels (lower left), and the water vapor mixing ratio (lnq) Jacobians (lower right).

network (NN) with numerous channels of BT as inputs and the matched-up wind profiles from ERA5 reanalysis as true values. NNs have shown significant ability to fit intricate nonlinear relationships between inputs and outputs through training and optimizations (Feng et al., 2017; LeCun et al., 2015; Van Gerven & Bohte, 2017), and have been successful in a number of meteorological applications with satellite observations (Boukabara et al., 2019; Milstein & Blackwell, 2016; Tao et al., 2018; Whitburn et al., 2016; Yao et al., 2019; Zhou & Grassotti, 2020). A feed-forward NN with an input layer, an output layer, and two hidden layers in between is used to retrieve the 3D U/V-wind profiles from hyperspectral observations from GIIRS. The inputs for NN consist of BTs of a specific FOV from 338 selected channels shown in Figure 1 at two consecutive observation times, both the current time and 15 min before. Also included are the two consecutive BT spectra of observations of the four FOVs surrounding the target FOV (neighbors in diagonal directions are not used to save computation), allowing spatial information to be included in the retrieval process. This ensures both the temporal and spatial variations of BTs from numerous channels are fed into the NN model. Each of the two hidden layers has 512 neurons, where the rectified linear activation function (Nair & Hinton, 2010) is applied in combination with He Initialization Scheme (He et al., 2015) before passing the results to the output layer where linear activation is applied to yield the outputs. The number of layers and neurons in hidden layers are decided on the basis of the rule-of-thumb methods concluded from previous research (Hagiwara, 1994; Karsoliya, 2012; Sheela & Deepa, 2013; Shibata & Ikeda, 2009; Tamura & Tateishi, 1997) along with some comparative tests, with retrieval accuracy, computational efficiency, and experimental simplicity all taken into consideration. For the output layer, there are 54 variables consisting of the U and V components of wind in 27 pressure levels from 100 to 1,000 hPa. The pressure levels are consistent with those of the ERA5.

The data set is first divided into a training set and an independent testing set. The scans starting at minute 00 of each hour are selected as testing data and not included in the training process, while the remaining three scans (starting at 15, 30, and 45 min) of each hour are included in the training set for developing the retrieval model. Then the training set is randomly separated into an 80% training subset and 20% validation subset, of which the former is used for training the model and the latter is for performance monitoring and model optimization. In the training process, the weights and biases are optimized through back-propagation with the usage of the Adam optimizer (Kingma & Ba, 2017) to minimize a loss function of mean squared error (MSE) between the predictions and the "truth" values. Early stopping based on the performance of validation set is applied along with L2 regularization (Girosi et al., 1995) to prevent overfitting issues (Glorot & Bengio, 2010). Then the performance of the model is evaluated using the independent testing set. Afterward, the results are further verified with wind products from other independent sources like GDAS analysis and dropsonde observations.

This ML based method is designed to statistically infer the nonlinear relationship between GEO hyperspectral IRS observations with spatial and temporal variations and the 4D wind fields without requiring formulation of the physical processes. As NN models have the capability of automatically extracting the useful information from the predictors through training, this method will not depend on any intermediate retrieval products (such as moisture) and avoid the uncertainties from the height assignment procedures when tracking moisture retrieval-based 3D AMVs.

3.3. Validation of Model Using Data Sets From Independent Sources

Independent NWP profiles from National Centers for Environmental Prediction Global Forecast System (GFS) short-range forecasts are also used to assess the potential added value from GIIRS 4D winds for future data assimilation. The GFS NWP data has 26 pressure levels in vertical from 10 to 1,000 hPa and a spatial resolution of 0.5° × 0.5°. It has a time interval of 3 h, with four initial forecast times a day at 0000, 0600, 1200, and 1800 UTC (Kalnay et al., 1990). For this investigation, we use the interpolated 3–12 h forecast data from the nearest initial forecast time as the benchmark for the evaluation.

Apart from ERA5 and NWP, the analysis data from the GDAS is used as another independent reference for output evaluation. The GDAS analysis has a spatial resolution of 0.25° × 0.25° and is distributed four times a day at 0000, 0600, 1200, and 1800 UTC as the gridded field to initialize the GFS model (Kanamitsu, 1989). For this investigation, the 3D wind profiles from 0600 and 1200 UTC are used as additional references to evaluate the retrievals from GIIRS. This will rule out the potential correlation effects from using the same type of data for training and validation.

In addition, the dropsonde profiles collected during Typhoon Maria, spatially and temporally collocated with GIIRS 4D winds are used as in situ measurements for validation. These dropsondes were released from a chartered flight to obtain the in situ observations. The dropsonde has equipped with sensors of GPS antenna, GPS receiver, pressure, temperature, and moisture. The data was transmitted back to the ground through satellite phone, followed the analysis and quality control (QC) procedure by using the Atmospheric Sounding Processing Environment software which is provided from University Corporation for Atmospheric Research. Thus, the 3D wind profile could be derived from the change of dropsonde in horizontal geolocations and altitudes while it's descending with the time. Similar data had been widely used in several studies, such as Chen et al. (2021) and Liu et al. (2020).

4. Results and Discussions

As mentioned in the previous section, a training data set and an independent testing data set are built up with spatially and temporally collocated GIIRS BTs and ERA5 U/V-wind profiles on 10 July 2018. Then QC is applied to remove FOVs with incomplete channel availability or unrealistic observation values (such as BT less than 100 K from any channel) and those FOVs located on the edges of the target area without enough neighboring FOVs. Considering that cloudiness in a FOV can directly affect GIIRS' capability of feature detection beneath the cloud, the samples are divided into three groups based on an averaged BT of 15 LW IR channels with wavelengths around 11 μm as follows:

1. Clear sky and very light cloud coverage (CRL): Fields-of-view (FOVs) with brightness temperature (BT) no less than 280 K. The sample sizes of the training and testing sets are 174,869 and 43,142, respectively;
2. Low and non-thick cloud coverage (LNT): FOVs with BT less than 280 K but no less than 240 K. The sample sizes of the training and testing sets are 96,459 and 23,606, respectively;
3. High and thick cloud coverage (HTK): FOVs with BT less than 240 K. The sample sizes of the training and testing sets are 29,502 and 6,598, respectively.

The training processes are carried out separately for each group. While the focus of our study lies on the clear sky and very light cloud coverage (CRL) group, a series of experiments are also carried out for the other groups to assess the impact of cloud coverage on the accuracy of wind retrievals from GIIRS.

4.1. Independent Validation Using ERA5

Shown in Figures 2a and 2b are the root mean squared errors (RMSEs) between the wind profiles from GIIRS retrievals and ERA5 of the three different groups, and those between the corresponding GFS forecasts and ERA5. Good agreement (relatively low RMSEs below 2 m/s for all the pressure levels) can be seen with GIIRS retrievals for the CRL and low and non-thick cloud coverage (LNT) groups; the GIIRS retrievals show smaller RMSEs than the GFS on most levels, except for the lower levels of LNT at 800 hPa and below. A possible reason for this may be that, when compared with upper levels dominated by free atmosphere, the accuracy of retrieval in boundary layer is limited due to the small contrast between near-surface radiation and surface radiation (Zeng, 1974), especially when clouds exist which would raise uncertainties in wind retrievals. Another reason is that the cloud coverage, though thin and low, would affect the capability of GIIRS in acquiring the information below the cloud. Such views are consistent with the performance of the high and thick cloud coverage (HTK) group, where the RMSE of GIIRS retrievals is much larger than GFS at all pressure levels below 150 hPa. It is worth noting that the GIIRS performance in the HTK group degrades significantly from that in the LTK group, while the GFS performance does not degrade as much. This is mainly due to the fact that high thick clouds block the infrared sounder from observing the atmosphere underneath the cloud, resulting in a lack of information for GIIRS to retrieve the wind profiles. Through QC, those HTK retrievals can be flagged out to avoid wind profiles over thick cloudy regions, especially the convective region.

Figure 2c shows the retrieved two-dimensional 200 hPa wind vectors of CRL FOVs on 1200 UTC from GIIRS (in green) and ERA5 (in red). The green arrows and red arrows in Figure 2c are well covered, indicating a high consistency between the retrieved wind fields from GIIRS and those from ERA5 analysis. As GIIRS green arrows cover the red arrows better compared with green arrows from NWP, it shows the potential of GIIRS observations to provide added value for NWP through data assimilation. A similar conclusion can be drawn from the comparison of 850 hPa winds from GIIRS retrievals (Figure 2e) and NWP (Figure 2f). Worth noting is that when the majority of FOVs show a better accuracy in GIIRS than NWP, the two clear FOVs that are located between the eyewall and outer rainbands show larger bias from GIIRS than NWP. Further research shows that when the current observations from window channels around 11 μm show an averaged BT of 283.05 K for these FOVs, the averaged BT for their neighboring FOVs are 271.84 K from current and 269.57 K from previous observations, respectively. It is similar for the FOVs in the eye area of typhoon, whose neighboring FOVs show an averaged BT 257.52 and 249.62 K, respectively, indicating that the degradation of accuracy is associated with cloud contamination from neighboring and previous observations. The time series of U and V components of wind from GIIRS and ERA5 at (113.1°E, 27.0°N) are shown in Figures 2g and 2h, respectively. This location is clear sky at all times and we only compared hourly data because ERA5 is hourly and the observations starting on the hour are used as independent testing. The general accuracy of retrieval is reasonable (mostly within 1 m/s) with some differences a little larger at 200 hPa.

Comparing the results from different cloud conditions and against GFS NWP, it appears that GIIRS high temporal data can be used to retrieve 4D wind profiles with reasonable accuracy and provide an added value to the wind profiles from GFS NWP background fields. A possible physical explanation is that when GIIRS is able to provide snapshot information of atmosphere with moisture distribution from MW radiances and thermodynamics from LW radiances, the temporal variations can give information on the movements of moisture and the thermal changes that are related to wind distributions, and the ML is able to utilize those
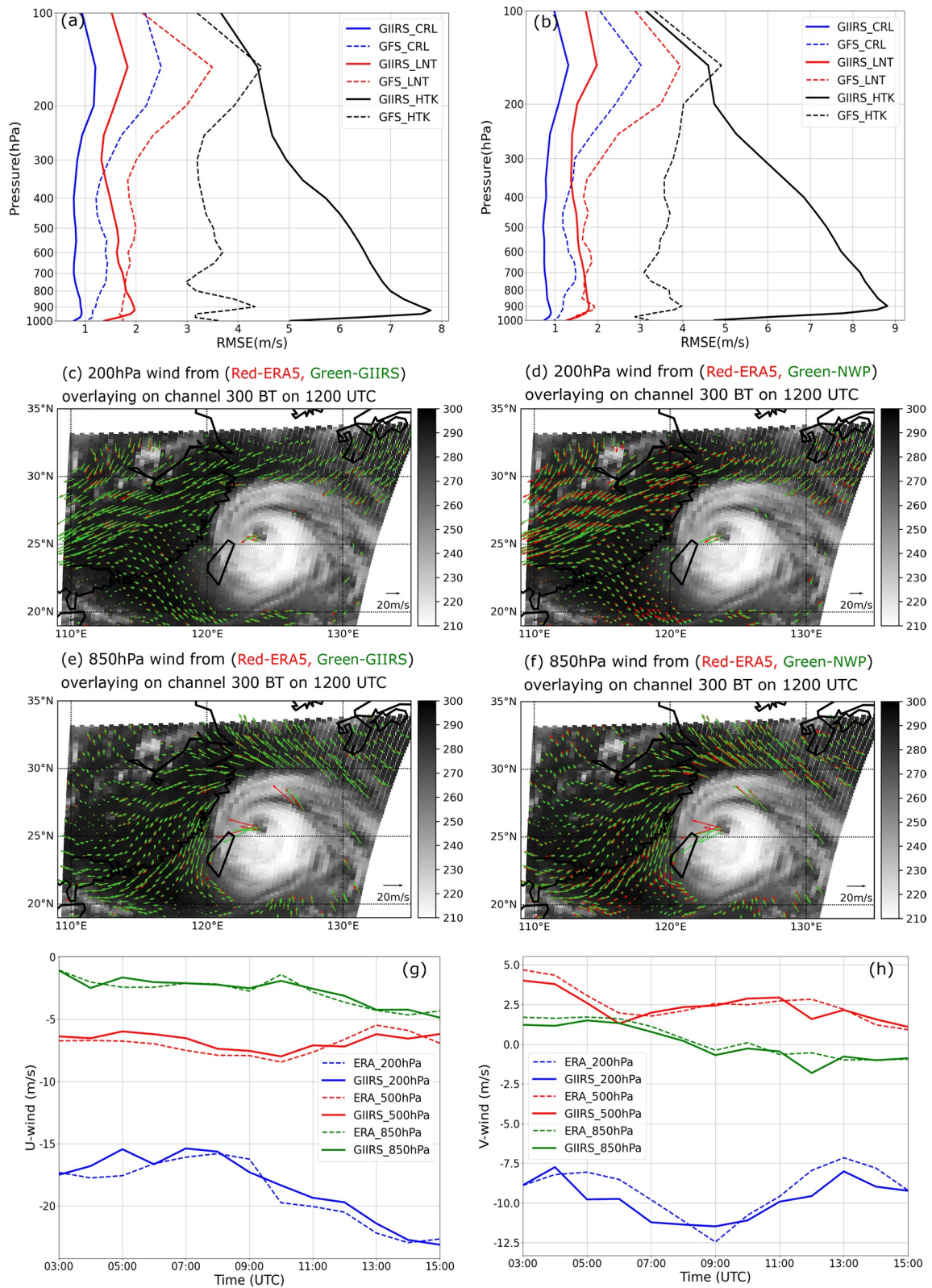
Figure 2

information and retrieve wind speeds. Also the variations of neighboring four FOVs can help determine the wind directions. However, the accuracy is significantly affected by cloud coverage and seriously degraded by high and thick clouds as the information from underneath is blocked by the clouds. This reveals that this ML based model retrieves the profiles from information of observations rather than pure correlations.

4.2. Independent Validation With GDAS Analysis and Dropsonde Data

In addition to the independent testing set from ERA5, it is always important to do further evaluations of the retrievals with other independent data sets. Shown in Figures 3a and 3b are statistical RMSEs among ERA5, GDAS, and GIIRS retrievals. The GDAS analysis only have products four times a day, our validation is carried out with available data from 0600 and 1200 UTC only. Shown in Figures 3a and 3b are the RMSEs of U and V among GIIRS retrievals, GDAS analysis, and ERA5, respectively. It can be seen that when the RMSE between GDAS and GIIRS retrievals appear to be larger than that between GIIRS and ERA5, the RMSE between GDAS and ERA5 lies in between and appear to be closer to the former one, inferring that the main source of the larger RMSE between GIIRS and GDAS comes from the difference between GDAS and ERA5. Since the model data are collocated from the exact same grid points, the difference is derived directly from model outputs. Despite such relative larger values than validations using ERA5, the values of RMSE lie in the range of 1–3 m/s, which still indicate reasonable accuracies for wind retrievals.

The wind retrieval results are also validated against dropsonde observations. Shown in Figures 3c and 3d are the vertical wind profile from dropsonde on 0006 UTC at (124.4°E, 24.4°N), compared with ERA5, GDAS, and retrieval results from GIIRS. The retrievals (depicted in blue lines) generally reproduced the pattern of soundings with reasonable accuracy, although some deviations can be seen on specific levels. This might be due to the differences in spatial and temporal as well as vertical resolutions between models and observation since the retrievals correspond better with ERA5 than the dropsonde. Similar results can be seen from Figures 3e and 3f showing the wind profiles on 1200 UTC at (114.2°E, 22.3°N). The general curves from dropsonde are well represented by the retrievals with good consistency with ERA5. However, some drastic changes displayed by the dropsonde profile are not shown by any other profiles, especially for the V-wind profiles. This is mainly due to the difference in vertical resolution between dropsonde and the gridded models like ERA5 and GDAS. When the GIIRS retrieval model is trained with ERA5 as the target profiles, it would be difficult for the ML based model to reproduce the additional curves that cannot be seen from ERA5.

5. Impact of Temporal and Spatial Information

As reasonable accuracy has been achieved with information on spatial and temporal variations included in the predictors of the ML based method, it is beneficial to further investigate how much that information contributes to the 4D wind retrievals. Additional experiments are carried out by replacing the GIIRS observations from 15 min before the current time with 30 and 60 min, to evaluate the impact on retrieval accuracy from temporal resolutions. Another experiment is conducted by using single FOV's observations as inputs, to evaluate the impact of spatial variations given from the neighboring FOVs on wind retrievals.

As is shown in Figures 4a and 4b, the result from experiments using 30 and 60 min as time intervals show larger RMSEs than the result from 15 min interval. As the interval increases from 30 to 60 min, the RMSEs become even larger, although the error is still acceptable. This indicates GIIRS observations with higher frequency, shorter time intervals, would result in higher accuracies of wind retrievals. A possible reason is that when GIIRS can provide information on moisture movements from MW radiances and thermodynamic variations from LW radiances, the values and distributions of their changing rates are related to the wind

Figure 2. Validation of wind retrievals from Geosynchronous Interferometric Infrared Sounder (GIIRS) against ERA5 analysis using the independent testing data set on 10 July 2018. The first row compares root mean squared error from GIIRS and Global Forecast System (GFS) for (a) U-component of wind; and (b) V-component of wind. The 200 hPa (second row) and 850 hPa (third row) wind fields using clear sky and very light cloud coverage fields-of-view from (c), (e) GIIRS and (d), (f) GFS numerical weather predictions (green arrows) are shown against ERA5 (red arrows) overlaying on the BT from channel 300 (wavenumber: 886.875 cm^{-1}) of GIIRS. The fourth row is for the comparison of time variations of (g) U-component of wind; and (h) V-component of wind at the location of (113.1°E, 27.0°N) from GIIRS and ERA5.
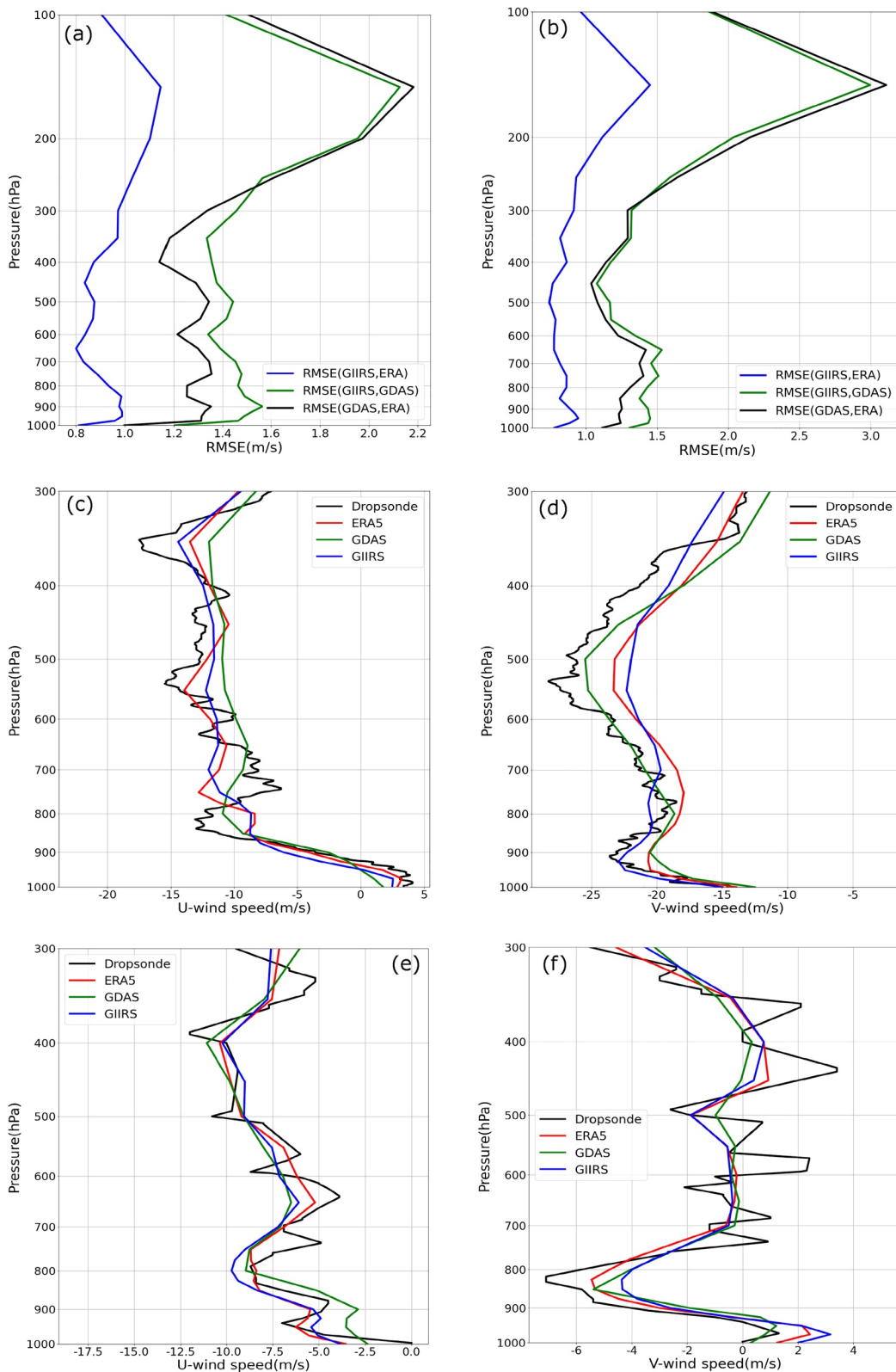
Figure 3. Comparison of root mean squared error of (a) U-component; and (b) V-component of wind from Geosynchronous Interferometric Infrared Sounder (GIIRS), ERA5 and Global Data Assimilation System (GDAS) using clear sky and very light cloud coverage samples on 0600 and 1200 UTC on 10 July 2018 (first row). Comparison of (c), (e) U-component; and (d), (f) V-component of wind profiles from GIIRS, ERA5, GDAS and dropsonde observations at (124.4°E, 24.4°N) on 0006 UTC (second row); and at (114.2°E, 22.3°N) on 1200 UTC (third row) on 10 July 2018.
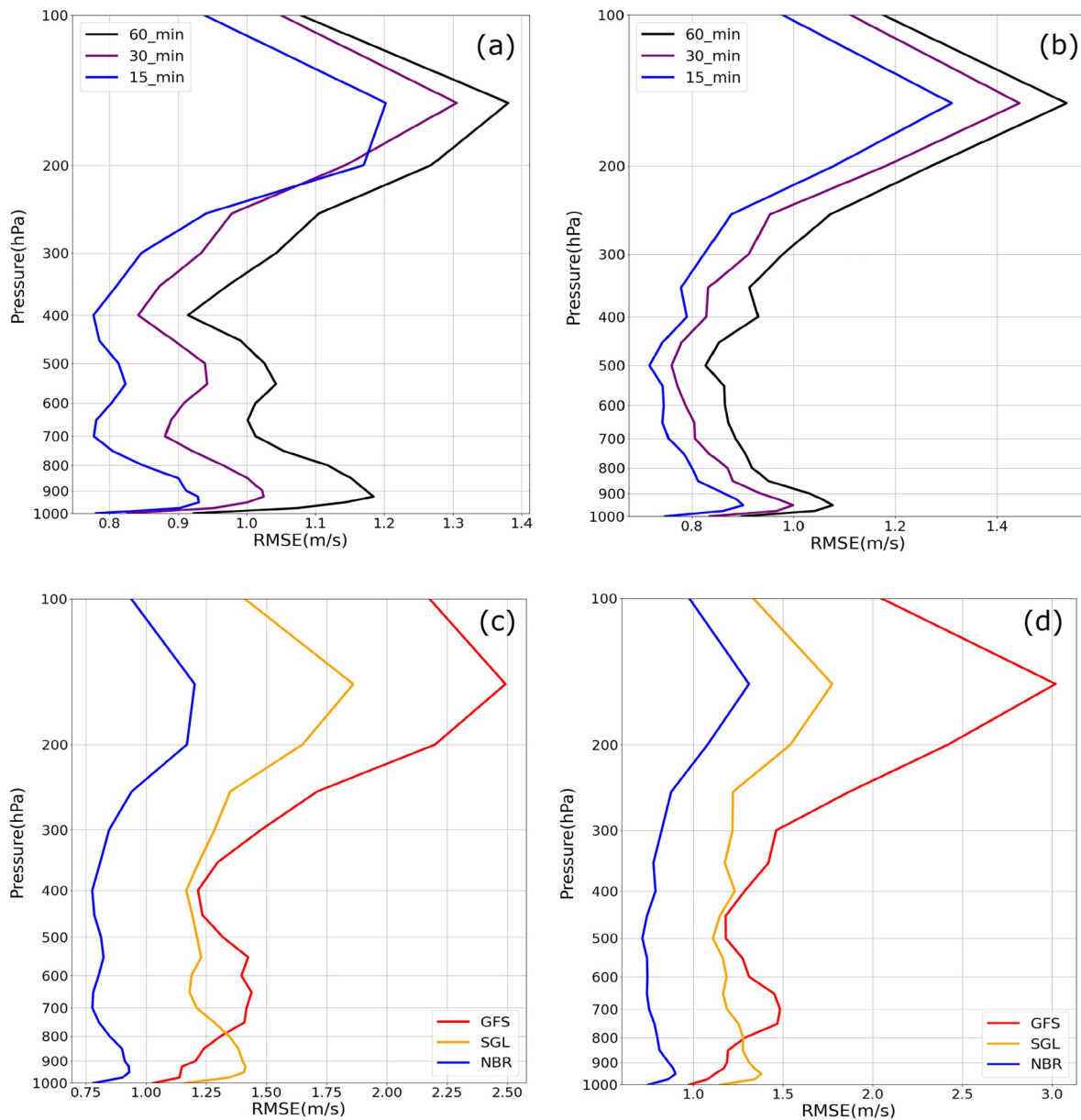
Figure 4. Comparison of root mean squared error profiles of (left column) U-component; and (right column) V-component of wind retrieved from model trained with different time intervals (upper row); and with single and neighboring fields-of-view included against numerical weather predictions from Global Forecast System on 10 July 2018.

vectors, thus a shorter time interval gives a better representativeness of the instantaneous changing rates and provides the retrievals with better accuracy.

Figures 4c and 4d show comparisons of U and V components of wind retrieved from single FOV (SGL, without neighboring FOVs) and with four neighboring FOVs included (NBR). An increase of RMSE is seen in SGL output compared with NBR, indicating a general positive contribution from the neighboring four FOVs on wind retrievals. It is worth noting that the retrievals from SGL also have comparable accuracy against ERA5 on the levels above 800 hPa, but the RMSEs appear larger than GFS in the boundary layer. This might be due to the degraded performance from tracking moisture in the boundary layer. With the neighboring observations included in the predictors, the information on horizontal variations of moisture and temperature which reflects atmospheric movement can be provided to the NN model and enhance the results via training.

6. Summary and Discussions

Four-dimensional wind profiles are derived from high-spectral resolution IR GIIRS radiances (BTs) with high temporal resolution of 15 min using ML based methodologies. The approach avoids the moisture profile retrieval and the associated errors in deriving the wind profiles as well as the height assignment. The main information comes from the moisture movement which is contained in the MW radiances from the two consecutive times, while the LW radiances help in conditioning the thermodynamic information related to wind distribution. Therefore, both LW and MW radiances are used for wind profile retrieval. The goal is to understand the value added from high temporal resolution GIIRS measurements to the NWP background, as well as to assess the independent information from GIIRS. Experiments with data from Typhoon Maria indicate that:

1. The four-dimensional (4D) wind field can be derived from high temporal resolution Geosynchronous Interferometric Infrared Sounder (GIIRS) measurements, when compared with independent numerical weather predictions background fields; added value can be seen as well.
2. The algorithm is applicable in clear and non-thick cloud skies. While for thick clouds, GIIRS might still provide useful information, considering the relatively large observation error under thick cloud skies. Further investigation is needed. The objective is to obtain 4D winds with as large as possible coverage while maintaining reasonable accuracy and precision.
3. The GIIRS 4D wind field reveals temporal variation similar to ERA5, indicating the unique value of geostationary hyperspectral measurements for providing dynamic information.
4. Higher temporal resolution provides better wind profile retrievals; this might be due to a better representativeness of the instantaneous variation of moisture movement and distribution that is essential for the three-dimensional wind retrievals. The spatial variation introduced by adding the neighboring radiances is important to assure good quality in the wind profile retrievals.

Ideally, a comparison between the ML method and the direct tracking should be carried out to better understand the potential of the former for wind retrieval from GIIRS. Unfortunately, such a comparison is not possible since there is no AMV product available using the direct tracking method from GIIRS. Instead, the AHI AMV products are used for the comparison to gain some insights. With ERA5 as reference, GIIRS wind with the DNN method has RMSE less than 1.5 m/s for both U and V for almost all levels in troposphere, while AHI AMV is mostly between 1.5 and 4 m/s. With GDAS as reference, similar results are obtained. GIIRS may improve the height assignment from the direct tracking with higher spectral resolution. The GIIRS with ML may overestimate the performance due to (a) the ERA5 used in both training and evaluation (although independently separated) are from the same meteorological case, and are therefore, not truly independent; and (b) there is only one day of such data. Without longer time period of data from more independent data sets, it is difficult to carry out comprehensive comparison of the two methods.

It should be noted that vertical velocity is not included in the algorithm, therefore, the 4D wind fields are horizontal winds at each pressure level and at each observation time. Whether the velocity can be derived from high temporal resolution geostationary hyperspectral IRS measurements is another research topic.

Although Typhoon Maria experiments show encouraging wind retrievals using high temporal resolution geostationary hyperspectral IR data, this study is still constrained by some limitations. First, the training data set is limited to a small data set, hence the representativeness of training not widely applicable. More comprehensive training data sets are needed. Unfortunately, 15-min data are only available for Typhon Maria so far. More studies and analysis are needed when additional 15-min interval data are available. Second, the coarser spatial resolution of GIIRS makes the algorithm difficult to use for detecting smaller tighter circulations. The spatial information is very important in tracking wind fields regardless of the methodology. With higher resolution anticipated in the future (e.g., GIIRS on FengYun-4B to be launched in 2021 which will have spatial resolution of 12 km, and IRS onboard MTG to be launched in 2023 will have 4 km spatial resolution), the spatial information will enable use in more sophisticated algorithms like convolutional neural network (Holmlund et al., 2021). Nevertheless, this study provides a practical scientific approach (from one-dimensional wind profile to 3D wind field) for deriving a 4D wind product from GEO hyperspectral IRS measurements with high temporal resolution, and demonstrates the importance of high temporal resolution from GEO. The study demonstrates that, in principle, 4D wind fields can be derived

from a geostationary hyperspectral sounder because of the dense temporal observation cycle, and provide added value for various quantitative applications such as NWP data assimilation, near real-time weather monitoring, situation awareness and nowcasting.

Data Availability Statement

GIIRS data were obtained from National Satellite Meteorological Center (NSMC) of China Meteorological Administration (CMA), and the GIIRS targeted observations for Typhoon Maria with 15 min temporal resolution are available: http://doi.org/10.5281/zenodo.4646464 (Han & Yin, 2021). ERA5 data were obtained from ECMWF at https://www.ecmwf.int/en/forecasts/datasets/reanalysis-datasets/era5. GFS and GDAS analysis were obtained from National Center for Environmental Information (NCEI) (https://www.ncdc.noaa.gov/data-access/model-data/model-datasets/global-data-assimilation-system-gdas). The raw dropsonde data were obtained from Taiwan's Central Weather Bureau, reprocessed for quality control version is available at http://doi.org/10.5281/zenodo.4671631 (Liu, 2021). The output wind products for Typhoon Maria can be found at http://doi.org/10.5281/zenodo.5048464 (Ma et al., 2021).

References

Boukabara, S.-A., Krasnopolsky, V., Stewart, J. Q., Maddy, E. S., Shahroudi, N., & Hoffman, R. N. (2019). Leveraging modern artificial intelligence for remote sensing and NWP: Benefits and challenges. *Bulletin of the American Meteorological Society*, *100*(12), ES473–ES491. https://doi.org/10.1175/BAMS-D-18-0324.1

Chen, S.-Y., Liu, C.-Y., Huang, C.-Y., Hsu, S.-C., Li, H.-W., Lin, P.-H., et al. (2021). An analysis study of FORMOSAT-7/COSMIC-2 radio occultation data in the troposphere. *Remote Sensing*, *13*(4), 717. https://doi.org/10.3390/rs13040717

Di, D., Li, J., Han, W., Bai, W., Wu, C., & Menzel, W. P. (2018). Enhancing the fast radiative transfer model for FengYun-4 GIIRS by using local training profiles. *Journal of Geophysical Research: Atmospheres*, *123*(22), 12–583. https://doi.org/10.1029/2018jd029089

Feng, Y., Peng, Y., Cui, N., Gong, D., & Zhang, K. (2017). Modeling reference evapotranspiration using extreme learning machine and generalized regression neural network only with temperature data. *Computers and Electronics in Agriculture*, *136*, 71–78. https://doi.org/10.1016/j.compag.2017.01.027

García-Pereda, J., & Borde, R. (2014). The impact of the tracer size and the temporal gap between images in the extraction of atmospheric motion vectors. *Journal of Atmospheric and Oceanic Technology*, *31*(8), 1761–1770. https://doi.org/10.1175/jtech-d-13-00235.1

Girosi, F., Jones, M., & Poggio, T. (1995). Regularization theory and neural networks architectures. *Neural Computation*, *7*(2), 219–269. https://doi.org/10.1162/neco.1995.7.2.219

Glorot, X., & Bengio, Y. (2010). Understanding the difficulty of training deep feedforward neural networks. In *Proceedings of the Thirteenth International Conference on Artificial Intelligence and Statistics* (pp. 249–256). JMLR Workshop and Conference Proceedings.

Graham, R. M., Hudson, S. R., & Maturilli, M. (2019). Improved performance of ERA5 in Arctic gateway relative to four global atmospheric reanalyzes. *Geophysical Research Letters*, *46*(11), 6138–6147. https://doi.org/10.1029/2019gl082781

Guo, Q., Yang, J., Wei, C., Chen, B., Wang, X., Han, C., et al. (2021). Spectrum calibration of the first hyperspectral infrared measurements from a geostationary platform: Method and preliminary assessment. *Quarterly Journal of the Royal Meteorological Society*, *147*(736), 1562–1583. https://doi.org/10.1002/qj.3981

Hagiwara, M. (1994). A simple and effective method for removal of hidden units and weights. *Neurocomputing*, *6*(2), 207–218. https://doi.org/10.1016/0925-2312(94)90055-8

Han, W., & Yin, R. (2021). FY-4A GIIRS targeted observations for Typhoon Maria (2018) with high temporal resolution of 15 minutes (Version 1.0) [Data set]. *Zenodo*. https://doi.org/10.5281/zenodo.4656877

He, K., Zhang, X., Ren, S., & Sun, J. (2015). Delving deep into rectifiers: Surpassing human-level performance on ImageNet classification. In *2015 IEEE International Conference on Computer Vision (ICCV)* (pp. 1026–1034). IEEE. https://doi.org/10.1109/ICCV.2015.123

Hersbach, H., Bell, B., Berrisford, P., Hirahara, S., Horányi, A., Muñoz-Sabater, J., et al. (2020). The ERA5 global reanalysis. *Quarterly Journal of the Royal Meteorological Society*, *146*(730), 1999–2049. https://doi.org/10.1002/qj.3803

Holmlund, K., Grandell, J., Schmetz, J., Stuhlmann, R., Bojkov, B., Munro, R., et al. (2021). Meteosat Third Generation (MTG): Continuation and innovation of observations from geostationary orbit. *Bulletin of the American Meteorological Society*, *102*(5), E990–E1015. https://doi.org/10.1175/bams-d-19-0304.1

Kalnay, E., Kanamitsu, M., & Baker, W. (1990). Global numerical weather prediction at the National Meteorological Center. *Bulletin of the American Meteorological Society*, *71*(10), 1410–1428. https://doi.org/10.1175/1520-0477(1990)071<1410:gnwpat>2.0.co;2

Kanamitsu, M. (1989). Description of the NMC global data assimilation and forecast system. *Weather and Forecasting*, *4*(3), 335–342. https://doi.org/10.1175/1520-0434(1989)004<0335:dotngd>2.0.co;2

Karsoliya, S. (2012). Approximating number of hidden layer neurons in multiple hidden layer BPNN architecture. *International Journal of Engineering Trends and Technology*, *4*.

Kingma, D. P., & Ba, J. (2017). *Adam: A method for stochastic optimization*. ArXiv:1412.6980 [Cs]. Retrieved from http://arxiv.org/abs/1412.6980

LeCun, Y., Bengio, Y., & Hinton, G. (2015). Deep learning. *Nature*, *521*(7553), 436–444. https://doi.org/10.1038/nature14539

Li, J., Li, J., Otkin, J., Schmit, T. J., & Liu, C.-Y. (2011). Warning information in a preconvection environment from the geostationary advanced infrared sounding system—A simulation study using the IHOP case. *Journal of Applied Meteorology and Climatology*, *50*(3), 776–783. https://doi.org/10.1175/2010JAMC2441.1

Li, J., Li, J., Velden, C., Wang, P., Schmit, T. J., & Sippel, J. (2020). Impact of rapid-scan-based dynamical information from GOES-16 on HWRF hurricane forecasts. *Journal of Geophysical Research: Atmospheres*, *125*(3). https://doi.org/10.1029/2019JD031647

Li, J., Liu, C.-Y., Zhang, P., & Schmit, T. J. (2012). Applications of full spatial resolution space-based advanced infrared soundings in the preconvection environment. *Weather and Forecasting*, *27*(2), 515–524. https://doi.org/10.1175/WAF-D-10-05057.1

Li, Z., Li, J., Wang, P., Lim, A., Li, J., Schmit, T. J., et al. (2018). Value-added impact of geostationary hyperspectral infrared sounders on local severe storm forecasts—Via a quick regional OSSE. *Advances in Atmospheric Sciences*, *35*(10), 1217–1230. https://doi.org/10.1007/s00376-018-8036-3

Liu, C.-Y. (2021). Dropsonde for TC Maria (2018) [Data set]. *Zenodo*. http://doi.org/10.5281/zenodo.4671631

Liu, C.-Y., Chiu, C.-H., Lin, P.-H., & Min, M. (2020). Comparison of cloud-top property retrievals from advanced himawari imager, MODIS, CloudSat/CPR, CALIPSO/CALIOP, and radiosonde. *Journal of Geophysical Research: Atmospheres*, *125*(15), e2020JD032683. https://doi.org/10.1029/2020jd032683

Ma, Z., Li, J., & Han, W. (2021). Four-dimensional wind fields retrieved from GIIRS hyperspectral measurements with 15-minute temporal resolution during Typhoon Maria (2018) [Data set]. *Zenodo*, https://doi.org/10.5281/zenodo.5048464

Menzel, W. P., Schmit, T. J., Zhang, P., & Li, J. (2018). Satellite-based atmospheric infrared sounder development and applications. *Bulletin of the American Meteorological Society*, *99*(3), 583–603. https://doi.org/10.1175/bams-d-16-0293.1

Milstein, A. B., & Blackwell, W. J. (2016). Neural network temperature and moisture retrieval algorithm validation for AIRS/AMSU and CrIS/ATMS. *Journal of Geophysical Research: Atmospheres*, *121*(4), 1414–1430. https://doi.org/10.1002/2015jd024008

Nair, V., & Hinton, G. E. (2010). Rectified linear units improve restricted Boltzmann machines. In *Proceedings of the 27th International Conference on Machine Learning (ICML-10)* (pp. 807–814).

Okamoto, K., Owada, H., Fujita, T., Kazumori, M., Otsuka, M., Seko, H., et al. (2020). Assessment of the potential impact of a hyperspectral infrared sounder on the himawari follow-on geostationary satellite. *SOLA-Scientific Online Letters on the Atmosphere*, *16*, 162–168. https://doi.org/10.2151/sola.2020-028

Olauson, J. (2018). ERA5: The new champion of wind power modeling? *Renewable Energy*, *126*, 322–331. https://doi.org/10.1016/j.renene.2018.03.056

Santek, D., Nebuda, S., & Stettner, D. (2019). Demonstration and evaluation of 3D winds generated by tracking features in moisture and ozone fields derived from AIRS sounding retrievals. *Remote Sensing*, *11*(22), 2597. https://doi.org/10.3390/rs11222597

Schmit, T. J., Li, J., Ackerman, S. A., & Gurka, J. J. (2009). High-spectral- and high-temporal-resolution infrared measurements from geostationary orbit. *Journal of Atmospheric and Oceanic Technology*, *26*(11), 2273–2292. https://doi.org/10.1175/2009JTECHA1248.1

Sheela, K. G., & Deepa, S. N. (2013). Review on methods to fix number of hidden neurons in neural networks. *Mathematical Problems in Engineering*, *2013*, 1–11. https://doi.org/10.1155/2013/425740

Shibata, K., & Ikeda, Y. (2009). Effect of number of hidden neurons on learning in large-scale layered neural networks. In *2009 IC-CAS-SICE* (pp. 5008–5013). IEEE.

Smith, W. L., Harrison, F. W., Hinton, D., Revercomb, H. E., Bingham, G., Petersen, R., & Dodge, J. (2002). GIFTS-the precursor geostationary satellite component of the future Earth Observing System. In *IEEE International Geoscience and Remote Sensing Symposium* (Vol. 1, pp. 357–361). IEEE.

Smith, W. L., Sr., Revercomb, H., Bingham, G., Larar, A., Huang, H., Zhou, D., et al. (2009). Evolution, current capabilities, and future advance in satellite nadir viewing ultra-spectral IR sounding of the lower atmosphere. *Atmospheric Chemistry and Physics*, *9*(15), 5563–5574. https://doi.org/10.5194/acp-9-5563-2009

Stettner, D., Velden, C., Rabin, R., Wanzong, S., Daniels, J., & Bresky, W. (2019). Development of enhanced vortex-scale atmospheric motion vectors for hurricane applications. *Remote Sensing*, *11*(17), 1981. https://doi.org/10.3390/rs11171981

Sun, F., Min, M., Qin, D., Wang, F., & Hu, J. (2018). Refined typhoon geometric center derived from a high spatiotemporal resolution geostationary satellite imaging system. *IEEE Geoscience and Remote Sensing Letters*, *16*(4), 499–503.

Szantai, A., Désalmand, F., Desbois, M., Lecomte, P., Perez, P., Zimeras, S., & Bouthemy, P. (2000). Tracking low-level clouds over land on Meteosat images. In *Proceedings of the Fifth International Winds Workshop, Lorne, Australia* (28 February–3 March 2000) (Vol. 28, pp. 245–252). EUMETSAT, EUM P.

Szantai, A., Héas, P., & Mémin, E. (2006). Comparison of atmospheric motion vectors and dense vector fields calculated from MSG images. In *Proceedings of the 8th International Winds Workshop* (pp. 24–28). Citeseer.

Tamura, S., & Tateishi, M. (1997). Capabilities of a four-layered feedforward neural network: Four layers versus three. *IEEE Transactions on Neural Networks*, *8*(2), 251–255. https://doi.org/10.1109/72.557662

Tao, Y., Hsu, K., Ihler, A., Gao, X., & Sorooshian, S. (2018). A two-stage deep neural network framework for precipitation estimation from bispectral satellite information. *Journal of Hydrometeorology*, *19*(2), 393–408. https://doi.org/10.1175/JHM-D-17-0077.1

Taszarek, M., Pilguj, N., Allen, J. T., Gensini, V., Brooks, H. E., & Szuster, P. (2020). Comparison of convective parameters derived from ERA5 and MERRA2 with rawinsonde data over Europe and North America. *Journal of Climate*, 1–55. https://doi.org/10.1175/jcli-d-20-0484.1

Van Gerven, M., & Bohte, S. (2017). Artificial neural networks as models of neural information processing. *Frontiers in Computational Neuroscience*, *11*, 114. https://doi.org/10.3389/fncom.2017.00114

Velden, C., & Bedka, K. M. (2009). Identifying the uncertainty in determining satellite-derived atmospheric motion vector height attribution. *Journal of Applied Meteorology and Climatology*, *48*(3), 450–463. https://doi.org/10.1175/2008JAMC1957.1

Velden, C., Daniels, J., Stettner, D., Santek, D., Key, J., Dunion, J., et al. (2005). Recent innovations in deriving tropospheric winds from meteorological satellites. *Bulletin of the American Meteorological Society*, *86*(2), 205–224. https://doi.org/10.1175/BAMS-86-2-205

Velden, C., Dengel, G., Dengel, R., Huang, A., Stettner, D., Revercomb, H., et al. (2004). Determination of wind vectors by tracking features on sequential moisture analyses derived from hyperspectral IR satellite soundings. In *Preprints, 13th AMS Conference on Satellite Meteorology and Oceanography*. American Meteorological Society. http://www.metvuw.com/courses/gphs424/pdf_conf_p42_s6_velden.pdf

Whitburn, S., Van Damme, M., Clarisse, L., Bauduin, S., Heald, C., Hadji-Lazaro, J., et al. (2016). A flexible and robust neural network IASI-NH3 retrieval algorithm. *Journal of Geophysical Research: Atmospheres*, *121*(11), 6581–6599. https://doi.org/10.1002/2016jd024828

Yang, J., Zhang, Z., Wei, C., Lu, F., & Guo, Q. (2017). Introducing the new generation of Chinese geostationary weather satellites, Fengyun-4. *Bulletin of the American Meteorological Society*, *98*(8), 1637–1658. https://doi.org/10.1175/BAMS-D-16-0065.1

Yao, Z., Li, J., Zhao, Z., Zhu, L., Qi, J., & Che, H. (2019). Extracting taklimakan dust parameters from AIRS with artificial neural network method. *Remote Sensing*, *11*(24), 2931. https://doi.org/10.3390/rs11242931

Yin, R., Han, W., Gao, Z., & Di, D. (2020). The evaluation of FY4A's Geostationary Interferometric Infrared Sounder (GIIRS) long-wave temperature sounding channels using the GRAPES global 4D-Var. *Quarterly Journal of the Royal Meteorological Society*, *146*(728), 1459–1476. https://doi.org/10.1002/qj.3746

Zeng, Q. C. (1974). *Principle of infrared remote sensing of atmosphere (in Chinese)* (p. 174). Science Press.

Zhang, S., Pu, Z., & Velden, C. (2018). Impact of enhanced atmospheric motion vectors on HWRF hurricane analyses and forecasts with different data assimilation configurations. *Monthly Weather Review*, *146*(5), 1549–1569. https://doi.org/10.1175/MWR-D-17-0136.1

Zhou, Y., & Grassotti, C. (2020). Development of a machine learning-based radiometric bias correction for NOAA's Microwave Integrated Retrieval System (MiRS). *Remote Sensing*, *12*(19), 3160. https://doi.org/10.3390/rs12193160